

Optimal design of DFG-based wavelength conversion based on hybrid genetic algorithm

Xueming Liu and Yanhe Li

Department of Electronic Engineering, Tsinghua University, Beijing, 100084, China

liuxueming72@yahoo.com

Abstract: A hybrid genetic algorithm (GA) is proposed. Simulating two test functions shows that the proposed GA can effectively solve the multimodal optimization problems, and the three movies demonstrate the detailed procedure of each generation. The conversion efficiency and bandwidth, based on quasi-phase-matching (QPM) difference frequency generation (DFG), are optimized by the matrix operator and our GA. Optimized examples for five-, six- and seven-segment QPM gratings are given, respectively. The optimal results show that adding the segment number of QPM can obviously broaden the conversion bandwidth, which is sensitive to the fluctuation of bandwidth and the variation of QPM grating period.

©2003 Optical Society of America

OCIS codes: (190.2620) Frequency conversion; (230.1150) All-optical devices; (000.5490) Probability theory, stochastic processes, and statistics.

References and links

1. X. M. Liu, H. Y. Zhang, Y. L. Guo, "Theoretical analyses and optimizations for wavelength conversion by quasi-phase-matching difference-frequency generation," *J. Lightwave Technol.* **19**, 1785-1792 (2001).
2. M. H. Chou, I. Brener, K. R. Parameswaran, M. M. Fejer, "Stability and bandwidth enhancement of difference frequency generation (DFM)-based wavelength conversion by pump detuning," *Electron. Lett.* **35**, 978-980 (1999).
3. X. M. Liu, H. Y. Zhang, and M. D. Zhang, "Exact analytical solutions and their applications for interacting waves in quadratic nonlinear medium," *Opt. Express* **10**, 83-97 (2002), <http://www.opticsexpress.org/abstract.cfm?URI=OPEX-10-1-83>
4. G. P. Banfi, P. K. Datta, V. Degiorgio, D. Fortusini, "Wavelength shifting and amplification of optical pulses through cascaded second-order processes in periodically poled lithium niobate," *Appl. Phys. Lett.* **73**, 136-138 (1998).
5. M.H.Chou, I.Brenner, G.Lenz, R.Scotti, E.E. Chaban, J.Shmulovich, D.Philen, S.Kosinski, K.R.parameswaran, and M.M.Fejer, "Efficient wide-band and tunable midspan spectral inverter using cascaded nonlinearities in LiNbO₃ waveguides," *IEEE Photon. Technol. Lett.* **12**, 82-84 (2000).
6. M. H. Chou, K. R. Parameswaran, M. M. Fejer, and I. Brener, "Multiple-channel wavelength conversion by use of engineered quasi-phase-matching structures in LiNbO₃ waveguides," *Opt. Lett.* **24**, 1157-1159 (1999).
7. X. M. Liu, H. Y. Zhang, Y. H. Li, "Optimal design for the quasi-phase-matching three-wave mixing," *Opt. Express* **9**, 631-636 (2001), <http://www.opticsexpress.org/oearchive/source/37804.htm>
8. M. H. Chou, J. Hauden, M. A. Arbore, I. Brener, M. M. Fejer, "1.5-um-band wavelength conversion based on difference-frequency generation in LiNbO₃ waveguides with integrated coupling structures," *Opt. Lett.* **23**, 1004-1006 (1998).
9. X. M. Liu, H. Y. Zhang, Y. L. Guo, Y. H. Li, "Optimal design and applications for quasi-phase-matching three-wave mixing," *IEEE J. Quantum Electron.* **38**, 1225-1233 (2002).
10. M. Asobe, O. Tadanaga, H. Miyazawa, Y. Nishida, H. Suzuki, "Multiple quasi-phase-matched LiNbO₃ wavelength converter with a continuously phase-modulated domain structure," *Opt. Lett.* **28**, 558-560 (2003).
11. T. Suhara, Y. Avetisyan, H. Ito, "Theoretical analysis of laterally emitting terahertz-wave generation by difference-frequency generation in channel waveguides," *IEEE J. Quantum Electron.* **39**, 166-171 (2003).
12. Y. Q. Qin, E. Wintner, "Optical filtering and switching using counter-propagating wavelength converter," *Opt. Quantum Electron.* **35**, 35-46 (2003).
13. M. C. Cardakli, A. B. Sahin, O. H. Adamczyk, A. E. Willner, K. R. Parameswaran, M. M. Fejer, "Wavelength conversion of subcarrier channels using difference frequency generation in a PPLN waveguide," *IEEE Photon. Technol. Lett.* **14**, 1327-1329 (2002).
14. D. Sato, T. Morita, T. Suhara, M. Fujimura, "Efficiency improvement by high-index cladding in LiNbO₃

- waveguide quasi-phase-matched wavelength converter for optical communication," *IEEE Photon. Technol. Lett.* **15**, 569-571 (2003).
15. W. Liu, J. Q. Sun, J. Kurz, "Bandwidth and tunability enhancement of wavelength conversion by quasi-phase-matching difference frequency generation," *Opt. Commun.* **216**, 239-246 (2003).
 16. M. H. Chou, I. Brener, M. M. Fejer, E. E. Chabass, and S. B. Christman, "1.5- μ m-band wavelength conversion based on cascaded second-order nonlinearity in LiNbO waveguides," *IEEE Photon. Technol. Lett.* **11**, 653-655 (1999).
 17. X. M. Liu and M. D. Zhang, "Theoretical studies for the special states of the cascaded quadratic nonlinear effects", *J. Opt. Soc. Am. B* **18**, 1659-1666 (2001).
 18. T. Suhara and H. Nishihara, "Theoretical analysis of waveguide second-harmonic generation phase matched with uniform and chirped gratings," *IEEE J. Quantum Electron.* **26**, 1265-1276 (1990).
 19. K. Mizuuchi, K. Yamamoto, M. Kato, and H. Sato, "Broadening of the phase-matching bandwidth in quasi-phase-matched second-harmonic generation," *IEEE J. Quantum Electron.* **30**, 1596-1604 (1994).
 20. K. Mizuuchi and K. Yamamoto, "Waveguide second-harmonic generation device with broadened flat quasi-phase-matching response by use of a grating structure with located phase shifts," *Opt. Lett.* **23**, 1880-1882 (1998).
 21. N. E. Yu, H. Ro, M. Cha, S. Kurimura, T. Taira, "Broadband quasi-phase-matched second-harmonic generation in MgO-doped periodically poled LiNbO₃ at the communications band," *Opt. Lett.* **27**, 1046-1048 (2002).
 22. X. L. Zeng, X. F. Chen, F. Wu, Y. P. Chen, Y. X. Xia, Y. L. Chen, "Second-harmonic generation with broadened flatband bandwidth in aperiodic domain-inverted gratings," *Opt. Commun.* **204**, 407-411 (2002).
 23. Y. Zhang, B. Y. Gu, "Optimal design of aperiodically poled lithium niobate crystals for multiple wavelengths parametric amplification," *Opt. Commun.* **192**, 417-425 (2001).
 24. B. Y. Gu, Y. Zhang, B. Z. Dong, "Investigations of harmonic generations in aperiodic optical superlattices," *J. Appl. Phys.* **87**, 7629-7637 (2000).
 25. J. Wu, T. Kondo, and R. Ito, "Optimal design for broadband quasi-phase-matched second-harmonic generation using simulated annealing", *J. Lightwave Technol.* **13**, 456-460 (1995).
 26. X. M. Liu, and B. Lee, "Optimal design of fiber Raman amplifier based on hybrid genetic algorithm," (submitted to *IEEE Photon. Technol. Lett.*)
 27. S. W. Mahfoud, "Niching methods for genetic algorithms," Ph.D. dissertation, Univ. of Illinois, Urbana-Champaign, 1995.
 28. X. M. Liu, and B. Lee, "Optimal design for ultrabroad-band amplifier," (submitted to *J. Lightwave Technol.*)
 29. S. W. Mahfoud, "Crowding and preselection revisited," In Manner, R., & Manderick, B. (Eds.), *Parallel Problem Solving from Nature* (Amsterdam, Elsevier Science, 1992) (pp. 27-36).
 30. B. L. Miller and M. J. Shaw, "Genetic algorithms with dynamic niche sharing for multimodal function optimization," in *Proc. 1996 IEEE Int. Conf. Evolutionary Computation*. Piscataway (NJ: IEEE Press, 1996).
 31. D. Thierens, D. E. Goldberg, "Elitist recombination: An integrated selection recombination GA," *Proceedings of the First IEEE Conference on Evolutionary Computation*, 1994, pp.508-512.
 32. Yin and N. Garmay, "A fast genetic algorithm with sharing scheme using cluster analysis methods in multimodal function optimization," in R. F. Albrecht, C. R. Reeves, and N. C. Steele, editors, *Proceedings of the International Conference on Artificial Neural Nets and Genetic Algorithms* (Berlin, Springer-Verlag, 1993).
 33. D. E. Goldberg, *Genetic Algorithms in Search, Optimization, and Machine Learning* (New York: Addison-Wesley, 1989).
 34. C. Y. Lin, W. H. Wu, "Niche identification techniques in multimodal genetic search with sharing scheme," *Adv. Eng. Software* **33**, 779-791 (2002).
 35. J. P. Li, M. E. Balazs, G. T. Parks, P. J. Clarkson, "A species conserving genetic algorithm for multimodal function optimization," *Evol. Comput.* **10**, 207-234 (2002).
 36. P. Siarry, A. Petrowski, M. Bessaou, "A multipopulation genetic algorithm aimed at multimodal optimization," *Adv. Eng. Software* **33**, 207-213 (2002).
 37. L. X. Guo, M. Y. Zhao, "A parallel search genetic algorithm based on multiple peak values and multiple rules," *J. Mater. Process Tech.* **129**, 539-544 (2002).
 38. K. Deb, A. Pratap, S. Agarwal, T. Meyarivan, "A fast and elitist multiobjective genetic algorithm: NSGA-II," *IEEE T. Evolut. Comput.* **6**, 182-197 (2002).
 39. R. B. Kasat, D. Kunzru, D. N. Saraf, S. K. Gupta, "Multiobjective optimization of industrial FCC units using elitist nondominated sorting genetic algorithm," *Ind. Eng. Chem. Res.* **41**, 4765-4776 (2002).
 40. J. K. Cochran, S. M. Horng, J. W. Fowler, "A multi-population genetic algorithm to solve multi-objective scheduling problems for parallel machines," *Comput. Oper. Res.* **30**, 1087-1102 (2003).
 41. R. Q. Lu, Z. Jin, "Formal ontology: Foundation of domain knowledge sharing and reusing," *J. Comput. Sci. Technol.* **17**, 535-548 (2002).
 42. L. Tamine, C. Chrisment, M. Boughanem, "Multiple query evaluation based on an enhanced genetic algorithm," *Inform. Process Manag.* **39**, 215-231 (2003).

43. J. Kivijarvi, P. Franti, O. Nevalainen, "Self-adaptive genetic algorithm for clustering," *J. Heuristics* **9**, 113-129 (2003).
44. K. G. Khoo, P. N. Suganthan, "Structural pattern recognition using genetic algorithms with specialized operators," *IEEE T. Syst. Man. Cy. B* **33**, 156-165 (2003).
45. J. M. Yang, C. J. Lin, C. Y. Kao, "A robust evolutionary algorithm for global optimization," *Eng. Optimize* **34**, 405-425 (2002).
46. X. H. Yuan, Y. B. Yuan, Y. C. Zhang, "A hybrid chaotic genetic algorithm for short-term hydro system scheduling," *Math. Comput. Simulat.* **59**, 319-327 (2002).
47. Z. Y. Wu, A. R. Simpson, "A self-adaptive boundary search genetic algorithm and its application to water distribution systems," *J. Hydraul. Res.* **40**, 191-203 (2002).
48. M. Kirley, "A cellular genetic algorithm with disturbances: Optimization using dynamic spatial interactions," *J. Heuristics* **8**, 321-342 (2002).

1. Introduction

All-optical wavelength conversion is widely recognized as a key technology for future wavelength division multiplexed (WDM) networks and as an important method of enhancing routing optical and network properties such as reconfigurability, nonblocking capability, and wavelength reuse. Among various strategies, quasi-phase-matching (QPM) wavelength converters based on difference frequency generation (DFG) or cascaded second-order nonlinear interactions have attracted much attention [1-17], because they offer potential advantages such as strict transparency, simultaneous multichannel conversion, wide bandwidth, high efficiency, and low noise. Efficient DFG-based wavelength conversion was realized in periodically poled LiNbO₃ waveguides [4-6]. In the experiments, a normalization conversion efficiency as high as 790%/W was obtained from a LiNbO₃ QPM-DFG device [14], and a fiber-to-fiber conversion efficiency of -8 dB was demonstrated by using cascaded nonlinear interactions [16].

In the uniform QPM grating, however, the conversion bandwidth is <90 nm for the nonlinear length $L > 25$ mm [1-3]. To broaden QPM bandwidth, all kinds of techniques were theoretically proposed and/or experimentally realized, e.g., chirped [18] and segmented [1, 7, 9, 19] grating method, phase shift method [9, 15, 20], pump detuning [2], multiple QPM [6,10] and employing nonlinear coefficient d_{31} [21]. To optimize QPM structure, the matrix operator [1,7,9] and simulated annealing method [22-25] were demonstrated.

Besides the simulated annealing method, the genetic algorithm (GA) also offers an effective global optimization method [26-48], which mimics the natural evolution and natural genetics. It has been successfully applied to finding the global optimum in a variety of unimodal domains. Unfortunately, a traditional-GA tends to converge towards a single solution and is even trapped in local optima of the search space due to selection pressure, selection noise, and operator disruption [27]. However, some problems require the identification of multiple optima in the domains. Although the simulated annealing method can avoid the local trap and find the global optimum, it fails to the multiple optima in the searching space. Fortunately, some methods such as clustering, sharing and crowding are proposed to extend the traditional-GA to solve multimodal function optimization by forcing a GA to maintain a diverse population of member throughout its research [26-48].

In this paper, we propose an effective hybrid GA, which includes such techniques as clustering, sharing, crowding, adaptive genetic operators, elitist replacement, and fitness scaling. Two test functions prove the proposed GA, and three simulation movies are also included. By means of our GA, DFG-based wavelength converters of nonuniform QPM grating structure are optimized.

2. Hybrid GA

The proposed GA is based on our previous GA in [26] and [28]. It not only improves the searching ability but also accelerates the convergence speed. The main procedure of the proposed GA is given as follows:

Step 0 (initialization): Initialize the number of peak centers n , the shortest niche radius r , the number of elitist set M and the number k . Generate N individuals randomly. Set the number of

generation, $g=1$. Go to *Step 6*.

Step 1 (clustering): Sort individuals according to the descending order of the fitness. Find out n peak centers (see *RULE I*). Allocate individuals to the nearest peak center (see *RULE II*).

RULE I: ① Assign the first individual as the first confirmed niche center, and mark it as *selected*. ② Select k (usually $k=n$) individuals orderly from the population, which satisfy the following conditions: the individuals are not marked as *selected*; the Euclidean distance from the individual to all of the confirmed peak centers is larger than r . ③ Calculate the sum of distances between each of k individuals and all of confirmed peak centers, assign the individual with the largest sum of distance as the next confirmed peak center, and mark it as *selected*. ④ Repeat ② and ③ until n peak centers are found.

RULE II: ① For each individual without being marked as *selected*, calculate its distances to n confirmed peak centers. ② Select the shortest distance and allocate the individual to the corresponding peak center. ③ Repeat ① and ② until N individuals are allocated.

Step 2 (sharing): Calculate the niche count m_i of each individual (m_i is equal to the individual count in each peak center). Calculate the shared fitness f'_i of an individual i , i.e., $f'_i=f_i/m_i$ (f_i is its genuine fitness). Each peak can be considered as a niche in the multimodal domain. Sharing, one of niching techniques, can maintain population diversity effectively.

Step 3 (selection): Perform a Roulette wheel selection scheme, which is the traditional selection function with the probability of surviving.

Step 4 (crossover): Implement a single-point crossover and employ an adaptive probability of crossover p_c , i.e.,

$$p_c = \begin{cases} p_{ch} - (p_{ch} - p_{cl})(f_{m2} - f_{ave})/(f_{max} - f_{ave}), & \text{if } f_{m2} > f_{ave}, \\ p_{ch}, & \text{otherwise} \end{cases}, \quad (1)$$

where f_{m2} is the maximum fitness of the two chromosomes being crossed, f_{max} and f_{ave} are the maximum fitness and average fitness of the entire population, and p_{ch} and p_{cl} are the probability of highest crossover and lowest crossover, respectively.

Step 5 (mutation): Implement a single mutation and employ an adaptive probability of mutation p_m , i.e.,

$$p_m = \begin{cases} p_{mh} - (p_{mh} - p_{ml})(f_{max} - f)/(f_{max} - f_{ave}), & \text{if } f > f_{ave}, \\ p_{mh}, & \text{otherwise} \end{cases}, \quad (2)$$

where f is the fitness of the chromosome, and p_{mh} and p_{ml} are the probability of the adaptive mutation, the highest mutation and the lowest mutation, respectively. $p_{ch}=0.99$, $p_{cl}=0.7$, $p_{mh}=0.02$ and $p_{ml}=0.005$ in this paper.

Step 6: Calculate the object value of each individual, and its corresponding fitness f .

Step 7 (crowding): If $g>2$, implement the deterministic crowding, which is described in [29].

Step 8 (elitist replacement): If $g>2$, replace M individuals of the population with the lowest fitness from the elitist set. If $g>1$, select M individuals as elitist set in order of fitness in each niche uniformly.

Step 9 (fitness scaling): Employ a linear scaling to scale the fitness function, i.e.,

$$f' = a \cdot f + b, \quad (3)$$

$$\begin{cases} a = (C_m - 1)f_{ave}(f_{max} - f_{ave}) \\ b = (f_{max} - C_m f_{ave})f_{ave}(f_{max} - f_{ave}) \end{cases}, \text{ if } f_{min} > \frac{C_m f_{ave} - f_{max}}{C_m - 1} \quad (4)$$

$$\begin{cases} a = f_{ave}(f_{ave} - f_{min}) \\ b = -a \cdot f_{min} \end{cases}, \text{ otherwise}$$

where C_m is a constant, and $C_m=1.2$ in our simulation; f_{min} is the minimum fitness of the entire population; other parameters are the same as Eqs. (1) and (2).

Step 10: If the terminating criteria is satisfied, then stop and output optimal results, else,

$g=g+1$ and go to *step 1*.

3. Matrix operator for QPM-DFG

Reference [9] shows that, although the propagation loss of the waveguide is sensitive to the conversion efficiency η , it is insensitive to the conversion bandwidth $\Delta\lambda$. In periodically poled crystal waveguides (e.g., LiNbO₃), the loss, group velocity mismatch, and dispersion of the material can normally be ignored for lengths $L\sim 20$ mm [6-10,19]. When the three waves propagate collinearly in a nonlinear medium with periodic structures (e.g., periodically poled LiNbO₃), each wave is coupled to the other two waves through the second-order nonlinear polarizability. This process is governed by the coupled-mode equations of QPM three-wave mixing, which can be derived from Maxwell's equations by invoking the slowly varying envelope approximation, and assuming a plane-wave interaction and a first-order diffraction effect of the grating perturbation [1,3,9,11,17-19]. Because the pump power is far greater than the signal and idler power, in the typical DFG process, the pump is regarded as undepleted (i.e., the small-signal approximation). By means of the matrix operator [1, 7, 9], the QPM-DFG process can be described as

$$\begin{bmatrix} E_1(L) \\ E_2^*(L) \end{bmatrix} = \begin{bmatrix} \mathbf{N}_1 & \mathbf{N}_2 \\ \mathbf{N}_3 & \mathbf{N}_4 \end{bmatrix} \begin{bmatrix} E_1(0) \\ E_2^*(0) \end{bmatrix}, \quad (5a)$$

$$\begin{bmatrix} \mathbf{N}_1 & \mathbf{N}_2 \\ \mathbf{N}_3 & \mathbf{N}_4 \end{bmatrix} = N_m N_{m-1} \dots N_1 \dots N_1, \quad (5b)$$

$$N_l = \begin{bmatrix} N_{l,1} & N_{l,2} \\ N_{l,3}^* & N_{l,1}^* \end{bmatrix}, l=1,2,\dots,m, \quad (5c)$$

$$N_{l,1} = \left[\cosh(Q_l L_l) + \frac{i\Delta k}{2Q_l} \sinh(Q_l L_l) \right] e_1, \quad (5d)$$

$$N_{l,2} = -i(M_1/Q_l) \sinh(Q_l L_l) e_2, \quad (5e)$$

$$N_{l,3} = -i(M_2/Q_l) \sinh(Q_l L_l) e_2, \quad (5f)$$

where $N_{l,2}^*$ and $N_{l,3}^*$ are the conjugate of $N_{l,2}$ and $N_{l,3}$, respectively, L_l is the length of the l -th segment (i.e., $L_l=z_l-z_{l-1}$), and z_{l-1} and z_l are the input and output places of this segment, respectively (See Fig. 1). $e_1=\exp(-i\Delta k_l L_l/2)$, $e_2=\exp(-i\Delta k_l(z_{l-1}+L_l)/2)$, and $Q_l = \sqrt{M_1 M_2^* - (\Delta k_l/2)^2}$ for the phase mismatching Δk_l of the l -th segment. $\Delta k_l=k_3-k_2-k_1-2\pi/\Lambda_l$ under the approximation of the first-order periodic perturbation effect. $M_j=\omega_j d_{eff} E_3(0)/(n_j c)$ ($j=1, 2$). Λ and c are the grating period and the speed of light in the vacuum, respectively. k_j , n_j and E_j are the wave vector, the index of refraction, and the electric field under light-frequencies ω_j ($j=1,2,3$; and ω_1 , ω_2 and ω_3 denote the signal, idler and pump waves), respectively. $E_3(0)$ is the electric field of pump at the input port (See Fig. 1).

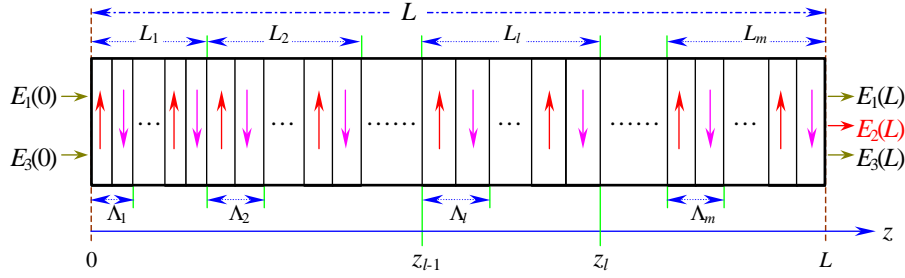


Fig.1. Model of nonuniform grating structure. Directions of the arrows represent those of the nonlinear coefficient. $E_2(L)$ accounts for the idler wave.

4. Test function

Real optimization problems often require the identification of multiple optima, either global or local or both. Our hybrid GA can maintain population diversity and permit it to investigate multiple peaks (including global and local) in parallel, and can prevent the GA from being trapped in local optima of the search space. To prove these points, we employ two multimodal functions of different difficulty. One test function is

$$y(x)=x+10\cdot\sin(5x)+7\cdot\cos(4x), \quad x\in[2.3, 5.8]. \quad (6)$$

This test function consists of three unequally spaced peaks with nonuniform height, which is demonstrated in Fig.2. Maxima are located at approximate x values of 2.9213, 4.1903, and 5.2468. Maxima are of approximate heights 16.2937, 9.3492, and 10.4057, respectively. Other test function is

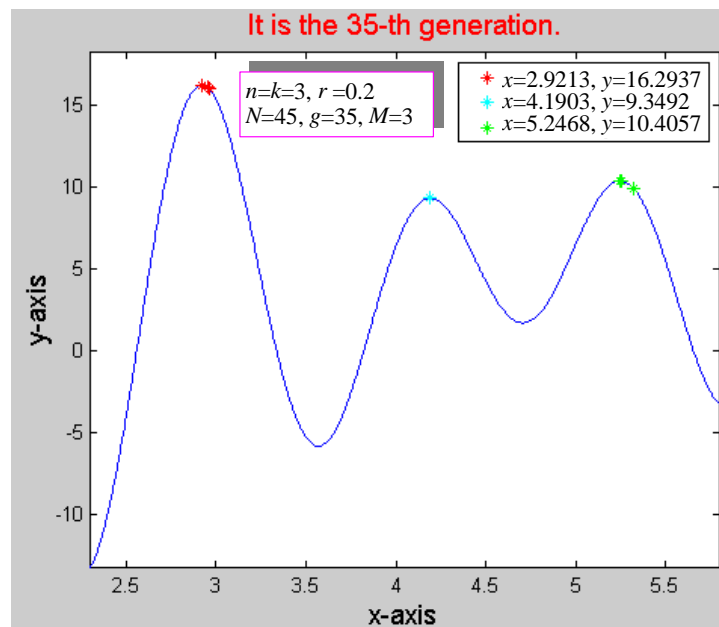
$$z(x, y) = \begin{cases} \frac{H_i}{R_i^2} \bar{R}^2 \left(\frac{\bar{R}^2}{R_i^2} - 2 \right) + H_i, & \text{if } \bar{R}^2 \leq R_i^2, x \in [0, 10] \text{ and } y \in [0, 10] \\ 0, & \text{otherwise} \end{cases} \quad (7)$$

where $\bar{R}^2 = X^2 + Y^2$, $X=x-x_{ci}$, $Y=y-y_{ci}$, $c_i=(x_{ci}, y_{ci})$, and $R_i=\{1.5, 2.5, 1, 0.75, 3\}$, $H_i=\{2, 4.4, 3, 4.5, 4\}$, $c_i=\{(2, 8), (3, 4), (5, 7), (7, 8.5), (7, 4)\}$. This test function consists of five peaks (center c_i , radius R_i and height H_i), which are displayed in Fig.3. The value of five peaks are 4.5 at (7, 8.5), 4.4 at (3, 4), 4 at (7, 4), 3 at (5, 7), and 2 at (2, 8). Fig.3 shows that the area of the second highest peak is much larger than that of the global peak and its local peak value of 4.4 is very close to the global peak value of 4.5. It results in the difficulty in finding the global peak without special technique.

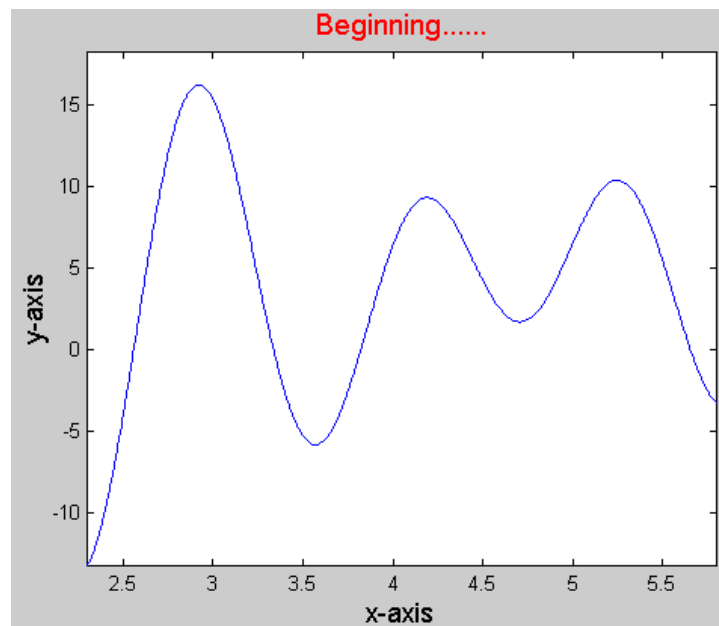
Each symbol “*” in Figs. 2 and 3 corresponds to each individual in the last generation of GA, and different color symbols in Figs. 2 and 3 represent the population of different peaks, respectively. In the simulation, $n=k=3$, $r=0.2$, $N=45$, $g=35$ and $M=3$ for Fig. 2; and $n=k=5$, $r=0.25$, $N=300$, $g=25$ and $M=50$ for Fig.3. Fig. 2(a) shows the curve of $y(x)$ and the distribution of all individuals in the 35-th generation, and Fig.2(b) demonstrates the procedure how our hybrid GA finds the global maximum and two local maxima of Eq. (6) in each generation. Fig. 3(a) exhibits the three-dimension figure of $z(x, y)$ and the distribution of all individuals in the 25-th generation, Fig. 3(b) illustrates the contour of $z(x, y)$ and the projection of all individuals of Fig. 3(a) in the xy -plane, and Fig. 3(c) and (d) demonstrate the procedure how our hybrid GA finds the global maximum and four local maxima of Eq. (7) in each generation.

In comparison with the traditional-GA, Figs. 2 and 3 show that our GA not only is able to find all peaks but also obviously accelerates the convergence speed. In fact, the traditional-GA usually finds the second highest peak of Fig. 3 instead of the global peak. Therefore, our proposed hybrid GA can effectively solve multimodal optimal questions and escape from

being trapped in local optima of the search space. Additionally, the numerical simulation also proves that the computing time T of our GA is obviously shortened in comparison with the traditional sharing GA. The reason is that $T \propto (kN)$ for our GA, but $T \propto (N^2)$ for the traditional sharing GA [27].



(a)



(b)

Fig. 2. Curve of $y(x)$ and the distribution of all individuals. (a) for the 35-th generation. (b) (298 KB) Film showing the procedure of each generation.

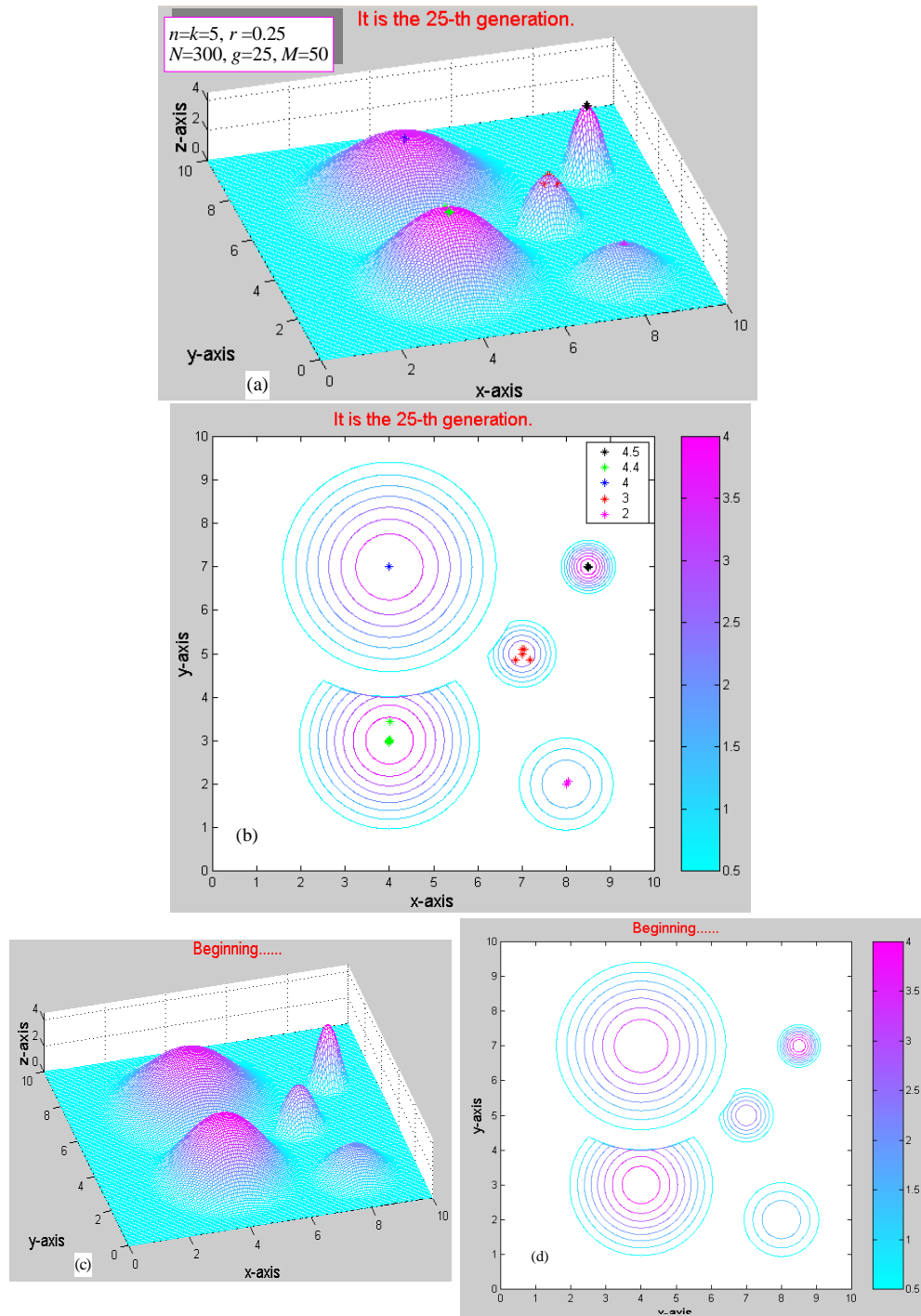


Fig. 3. Test function $z(x, y)$ and the entire population in the 25-th generation. (a) For the three-dimension figure of $z(x, y)$ and the distribution of all individuals. (b) For the contour of $z(x, y)$ and the projection of all individuals of (a) in the xy -plane. (c) (1120 KB) Film showing the procedure of each generation in the three-dimension figure. (d) (1193 KB) Film showing the procedure of each generation in the contour of $z(x, y)$. Five different color symbols represent the population of five peaks, respectively.

5. Optimized results by means of hybrid GA

Although two-, three-, and four-segment QPM structures were optimized by the exhaustion method in [1, 9], more effective algorithms have to be implemented when the segment number $m \geq 5$. Fortunately, our proposed GA can availablely overcome these difficulties. In the simulation calculations, we employ the representative data of periodically poled LiNbO₃ [1, 3, 9, 17]: the pump power $P_3=200$ mW and wavelength $\lambda_3=775$ nm; $d_{eff}=15$ pm/V and $L=20$ mm; the signal channels spaced 1 nm/channel are from 1440 nm to 1660 nm, and each input signal power $P_1=1$ mW; the effective channel waveguide cross section is $30\mu\text{m}^2$; the lengths of all segments are assumed to be equal, i.e., $L_1=L_2=\dots=L_m$. The relation between the light intensity I and the electric field E is that $I=\epsilon_0cn|E|^2/2$, and ϵ_0 is the dielectric permittivity in the vacuum. Additionally, $N=1500$, $M=150$, $n=k=5$, $g=100$ and $r=0.1$ (here r is the normalized Euclidean distance).

Figures 4 (a)-(c) show the optimal results of the conversion efficiency η and its corresponding bandwidth $\Delta\lambda$ versus the signal wavelength λ_1 in five-, six- and seven-segment structures, respectively. Their corresponding optimal values of Λ are tabularized in tables 1-3. p_l ($l=1, 2, \dots, 5$) in figures and tables represents the l -th peak center, and $\Delta\lambda$ is the corresponding optimal conversion bandwidth. In the optimal simulation of Tables 1-3 and Fig. 4, we assume that: the conversion efficiency is >-6 dB, the fluctuation of the conversion bandwidth is <1 dB; and The variation of the grating period Λ is 1 nm [see Fig. 4 (a)].

It is easily seen, from Tables 1-3 and Fig. 4, that ① the optimal bandwidth $\Delta\lambda$ is broadened with an increase in the segment number m , e.g., $\Delta\lambda=192$ nm for seven segments against $\Delta\lambda=150$ nm for five segments; ② there are the same or approximately the same $\Delta\lambda$ for each peak center for a given segment number; ③ to realize the fixed $\Delta\lambda$ in the experiments, therefore, there are several candidates by the optimization of our GA, and this result has important applications in the design of QPM structure; ④ our proposed GA can effectively avoid the local trap during the optimal procedure; ⑤ the global maximum value $\Delta\lambda$ lies in the first peak center p_1 , as is determined in the assumption of our GA.

Table 1. Optimized Bandwidth $\Delta\lambda$ for Five-Segment QPM structure

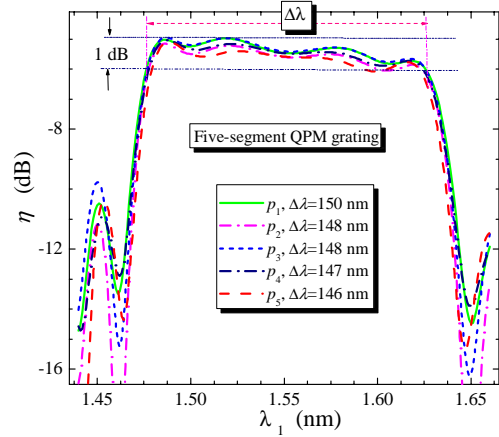
	Λ_1 (μm)	Λ_2 (μm)	Λ_3 (μm)	Λ_4 (μm)	Λ_5 (μm)	$\Delta\lambda$ (nm)
p_1	16.211	16.215	16.217	16.218	16.240	150
p_2	16.242	16.205	16.209	16.212	16.214	148
p_3	16.211	16.217	16.217	16.218	16.240	148
p_4	16.208	16.213	16.216	16.217	16.239	147
p_5	16.225	16.218	16.218	16.200	16.240	146

Table 2. Optimized Bandwidth $\Delta\lambda$ for Six-Segment QPM structure

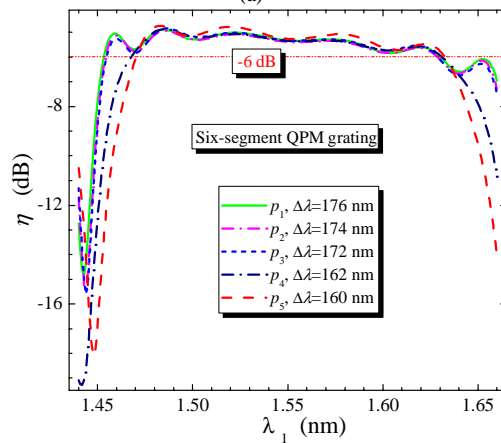
	Λ_1 (μm)	Λ_2 (μm)	Λ_3 (μm)	Λ_4 (μm)	Λ_5 (μm)	Λ_6 (μm)	$\Delta\lambda$ (nm)
p_1	16.213	16.204	16.212	16.215	16.219	16.239	176
p_2	16.216	16.204	16.213	16.215	16.219	16.239	174
p_3	16.217	16.205	16.214	16.215	16.219	16.239	173
p_4	16.240	16.197	16.237	16.212	16.196	16.183	162
p_5	16.214	16.244	16.235	16.231	16.248	16.197	160

Table 3. Optimized Bandwidth $\Delta\lambda$ for Seven-Segment QPM structure

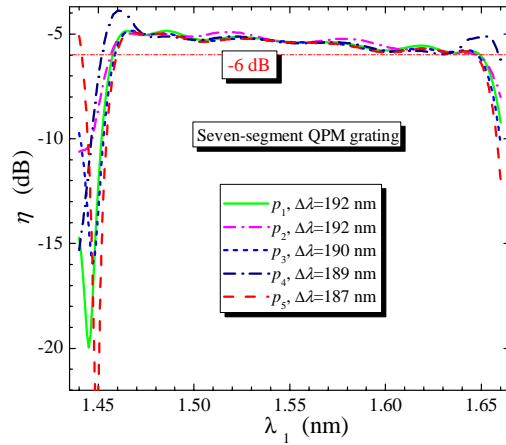
	Λ_1 (μm)	Λ_2 (μm)	Λ_3 (μm)	Λ_4 (μm)	Λ_5 (μm)	Λ_6 (μm)	Λ_7 (μm)	$\Delta\lambda$ (nm)
p_1	16.223	16.250	16.234	16.236	16.253	16.246	16.210	192
p_2	16.194	16.239	16.232	16.208	16.191	16.245	16.195	192
p_3	16.230	16.185	16.239	16.236	16.211	16.230	16.238	190
p_4	16.237	16.189	16.239	16.238	16.194	16.197	16.197	189
p_5	16.235	16.202	16.213	16.217	16.235	16.187	16.253	187



(a)



(b)



(c)

Fig. 4. Optimal results for the conversion efficiency η and bandwidth $\Delta\lambda$ of signal wavelength λ_1 in five-, six-, and seven-segment QPM grating: (a) five-segment, (b) six-segment, and (c) seven-segment. η is assumed to be >-6 dB, the fluctuation of $\Delta\lambda$ is <1 dB, and the variation in the grating period Λ is 1 nm.

Although Tables 1-3 and Fig. 4 are obtained from Eq. (5), which is valid under the condition of loss free (corresponding nonlinear length $L < 20$ mm [9]), the optimized conversion bandwidth $\Delta\lambda$ is still right by use of Eq. (5) when the waveguide loss is taken into account for $20 < L < 50$ mm. But, for this case, the conversion efficiency η decreases. These results are consistent with [9]. The reasons are that, with the waveguide loss, the depletion of signals and pumps leads to the decrease of converted waves, and the approximately same decrease of signals and converted waves makes $\Delta\lambda$ be almost unchanged. For the practicable design of QPM devices, the experimental conditions limit the variation of Λ and the tolerance of phase mismatch. In the following parts, we give an example under the condition of the Λ variation of 10 nm instead of 1 nm. Of course, our proposed algorithm can effectively optimize the nonuniform QPM grating structures at any value of the Λ variations.

To clearly understand the relationships of the conversion efficiency η and bandwidth $\Delta\lambda$ with the fluctuation of $\Delta\lambda$ and the variation of Λ , we give two optimized examples for η and $\Delta\lambda$ versus λ_1 under the conditions of the $\Delta\lambda$ fluctuation of < 2 nm and the Λ variation of 10 nm in five-segment QPM structure, respectively. The optimized results are illustrated in Fig. 5. By comparing Fig. 4(a) with Fig. 5, it is found that ① $\Delta\lambda = 168$ nm in the $\Delta\lambda$ fluctuation of < 2 nm against $\Delta\lambda = 150$ nm in that of < 1 nm and ② $\Delta\lambda$ decreases from 150 nm to 117 nm when the variation of Λ is from 1 nm to 10 nm under the same other conditions. The simulated results also show that ① improving the property of the $\Delta\lambda$ fluctuation (i.e., decreasing the $\Delta\lambda$ fluctuation) is at the cost of narrowing the conversion bandwidth $\Delta\lambda$ and ② extending the variation of Λ also makes $\Delta\lambda$ narrowed.

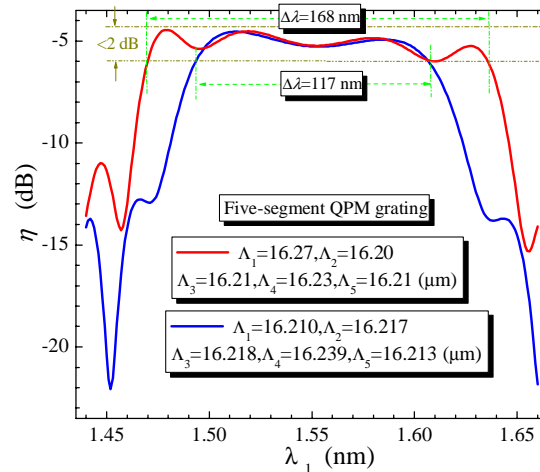


Fig. 5. Optimal results for the conversion efficiency η and bandwidth $\Delta\lambda$ of signal wavelength λ_1 in five-segment QPM grating: Red and blue curves account for the $\Delta\lambda$ fluctuation of < 2 nm and the Λ variation of 10 nm, respectively. Other parameters and assumptions in Fig. 5 are consistent with those in Fig. 4(a).

Although Figs. 4 and 5 and Tables 1-3 only denote some specific examples, e.g., five-, six-, and seven-segment QPM grating structures, our proposed hybrid GA can provide powerful tool for all kinds of the nonuniform QPM grating structures. In virtue of the inherent merits of GA [27, 33], our GA can be implemented into all sorts of practical tolerances and requirements after little modification. Therefore, our proposed GA can effectively offer the optimal tool for the practical design of QPM grating under the determinate conditions.

6. Conclusions

In the paper, we have proposed a hybrid GA, which includes such techniques as clustering, sharing, crowding, adaptive genetic operators, elitist replacement, and fitness scaling. Simulating two test functions shows that our GA can obtain the global and all local peak values

in parallel, and three movies demonstrate the detailed procedure of each generation. By means of the matrix operator and hybrid GA, DFG-based wavelength converters in nonuniform QPM grating structures are optimized. Three examples (i.e., five-, six- and seven-segment QPM gratings) and five peak values are obtained in parallel, respectively. The optimal results show that ① increasing the segment number of QPM grating can availablely broaden the conversion bandwidth $\Delta\lambda$, ② decreasing the fluctuation of $\Delta\lambda$ (i.e., improving the properties of the fluctuation of $\Delta\lambda$) is at the cost of $\Delta\lambda$, e.g., $\Delta\lambda=168$ nm in the $\Delta\lambda$ fluctuation of <2 nm against $\Delta\lambda=150$ nm in that of <1 nm, and ③ extending the variation of Λ decreases $\Delta\lambda$, e.g., $\Delta\lambda=150$ nm in the Λ variation of 1 nm against $\Delta\lambda=117$ nm in that of 10 nm. Our proposed GA has important applications in the practical design of nonuniform QPM grating structure.

Acknowledgment

This work was supported by the National Natural Science Foundation of China (60132020). The authors would like to thank Dr. Xin-Jun Liu and Dr. Xinjie Yu, Tsinghua Univ., for helping to make three movies and fruitful discussions on the GA, respectively.

Xueming Liu is currently engaged in postdoctoral work at School of Electrical Engineering, Seoul National University, Seoul 151-744, Korea.